Journal of Crystal Growth 311 (2009) 3889–3897

Contents lists available at ScienceDirect

Journal of Crystal Growth

journal homepage: www.elsevier.com/locate/jcrysgro

Precursor-controlled synthesis of hierarchical ZnO nanostructures, using oligoaniline-coated Au nanoparticle seeds

Deepti Krishnan, T. Pradeep *

DST Unit on Nanoscience (DST UNS), Department of Chemistry and Sophisticated Analytical Instrument Facility, Indian Institute of Technology Madras, Chennai 600 036, India

ARTICLE INFO

Article history:
Received 6 May 2009
Received in revised form
26 May 2009
Accepted 9 June 2009
Communicated by K. Nakajima
Available online 18 June 2009

PACS:
61.46.−w
61.46.Df
81.10.Aj
68.37.Lp
68.37.−d

Keywords:
A1. Crystal morphology
A1. Nucleation
A2. Growth from solutions
B1. Zinc compounds
B2. Semiconducting II–VI materials

ABSTRACT

Shape-selected synthesis of a large number of zinc oxide (ZnO) nano- and microstructures was achieved by the seed-mediated growth of oligoaniline-coated gold nanoparticle precursors. Distinctive ZnO structures such as nanoplates, nanospheres, microstars, microflowers, microthorns and micromultipods were synthesized by this method. Slightly different shapes were obtained in the absence of the seed solution. This is a fast, low temperature (60 °C) and biomimetic route to make a wide variety of structures. The structure and morphology of the nanostructures were studied by transmission electron microscopy (TEM) and scanning electron microscopy (SEM), respectively. Raman spectroscopy, Fourier-transform infrared (FTIR) spectroscopy and X-ray diffraction (XRD) were utilized for the characterization of the nanostructures. A growth mechanism for these nanostructures was proposed based on these results. The concentrations of the reacting species were the main parameter causing the changes in the morphologies. The variation in morphologies of these structures is believed to be due to the ability of the seed solution as well as polyvinylpyrrolidone (PVP) to selectively suppress/depress the growth of certain planes, allowing growth to occur only in certain specific directions. Changes in the amount of growth nuclei with varying sodium hydroxide (NaOH) concentration is also seen to affect the morphology of these structures.

1. Introduction

Zinc oxide (ZnO), a semiconductor with a direct wide band gap (3.37 eV–387 nm, deep violet/borderline ultraviolet (UV)) and a large exciton-binding energy (60 meV) [1], is a highly preferred multitasking metal oxide having a vast list of attractive properties. Due to its unique optical and electrical properties [2,3], it is regarded as a potential material in optoelectronic applications operating in the visible and near ultraviolet spectral regions. The areas in which it is used include, UV light-emitting diodes [4–6], nanolasers [7], gas sensors [8], highly-efficient green phosphors [9], photo-catalysts and photovoltaic devices [10,11], field-effect transistors [12], chemical sensors [13], transparent conductors and varistors [14,15]. Also it possesses excellent thermal and chemical stability, a large piezoelectric coefficient, and an easily modifiable electrical conductivity. It is non-toxic, compatible with skin, antimicrobial and is used as an UV-blocker in sunscreens.

The tremendous interest in ZnO is due to its unique ability of possessing structure-dependent properties. Properties like electrical and thermal transport, in addition to optical and mechanical properties, could be varied with respect to particle size, shape, morphology, orientation and aspect ratio. Hence, morphology and dimensionality-controlled growth of zinc oxide has become a challenging topic lately to design novel functional devices. So far, numerous nanostructured ZnO's with various morphologies have been fabricated like plates [16], wires [17], belts [18], rods [19], pyramids [20], cages and shells [21], dandelions [22], branched crystallites [23], organic-capped nanocrystals [24], urchins [25], hollow spheres [26], bridges and nails [27], hemispherical bowls [28], ellipsoids and nanocolumns [29], towers [30], cones and reefs [31] and stars [32]. The most common routes for preparing these structures fall into either vapor-phase synthesis [33–41] such as vapor-liquid-solid (VLS) growth, chemical vapor deposition (CVD), metal organic chemical vapor deposition (MOCVD), thermal decomposition and thermal evaporation or solution-phase synthesis [42,43] like hydrothermal, microemulsion and template-assisted sol–gel processes. Among the two categories, solution-phase techniques are highly preferred as they involve low temperature and are cheaper for scale-up. Vapor-phase techniques require high temperature (of more than 250 °C) and are expensive, besides demand stringent conditions. Hence, it is highly desirable to develop a synthesis which requires mild conditions, due to its easy incorporation in biologically relevant processes as well as in practical applications.

* Corresponding author. Tel.: +8175753 5445/+91 44 2257 4208; fax: +91 44 2257 0545.
E-mail address: pradeep@iitm.ac.in (T. Pradeep).

0022-0248/$ - see front matter © 2009 Elsevier B.V. All rights reserved.
doi:10.1016/j.jcrysgro.2009.06.019

Herein, we report a simple, biomimetic and low-temperature method for the fabrication of ZnO nanostructures such as plates, spheres, stars, flowers and multipods in the presence of polyvinylpyrrolidone (PVP), using Au-oligoaniline as the seed. Gold/polyaniline (Au/PANI) as a precursor has been known to give star-shaped Au nanostructures [44]. Though reports exist on the synthesis of Au@ZnO composites by solution-phase method [45], no attempts have been reported till date for the synthesis of ZnO of varying morphologies using Au-containing seeds. Experiments were also conducted to see the different shapes obtained in the absence of seed solution using the commonly used bio-friendly template, PVP. All the nanostructures attained were characterized using various spectroscopic and microscopic techniques and a possible mechanism for the formation of these morphologies is proposed.

2. Experimental process

2.1. Materials

Aniline was purchased from Sigma Aldrich and distilled twice under reduced pressure before use. Zinc acetate ($(CH_3COO)_2Zn$) and sodium hydroxide (NaOH) were purchased from Ranbaxy. PVP was purchased from Merck. Tetrachloroauric acid trihydrate ($HAuCl_4 \cdot 3H_2O$) was purchased from CDH, India. All chemicals were used as such without further purification. Triply distilled water was used throughout the experiments. Scheme 1 shows the experimental procedure employed for making various nanostructures using Au/PANI seed solution.

Synthesis involves the following steps.

2.2. Synthesis of oligoaniline-coated gold nanoparticles (AuNPs)

Au/PANI has been synthesized by a known procedure described by Sajanlal et al. [44]. In a typical synthesis, 25 mg of citric acid was dissolved in 35 mL of water. The solution was kept at 80 °C and 1 mL of 25 mM $HAuCl_4$ was added. After 10 min, when the color changed from pale yellow to pink, 100 μL distilled aniline was added followed by 500 μL 25 mM $HAuCl_4$. Heating was continued for five more minutes. The color of the solution changed to light pink and a black precipitate was formed. This solution was kept at room temperature for 5 h, centrifuged at 4000 rpm and the black residue was discarded. The resultant light pink supernatant, which contains oligoaniline-capped gold nanoparticles, was used for further reaction.

2.3. Synthesis of ZnO nanostructures

A total of 1 mL of the above-prepared seed solution was heated in a 20 mL sample bottle at 60 °C. To it, 10 mL of aqueous PVP (12.5 mg/mL) was added without varying the temperature. After 30 s, 1 mL of zinc acetate was added, followed by the addition of 1 mL NaOH of required concentration, so as to maintain a particular Zn^{2+}:OH^- ratio. Heating was continued for 1 h to get a clear supernatant with white precipitate at the bottom of the bottle. The supernatant was removed and the white precipitate was washed a couple of times with both ethanol and water. Finally it was kept for drying at 80 °C for 4 h in an oven and the white powder thus obtained was used for subsequent analysis. The experiment was conducted at different ratios of Zn^{2+}:OH^-, such as 1:0.8, 1:1.75, 1:3, 1:5, 1:7.5 and 1:40 to get nano-hexagonal plates, nano-oval plates, micro-stars, micro-flowers, thorns and multipods, respectively. Scheme 1 gives a schematic of the synthetic procedure.

2.4. Instrumentation

Transmission electron microscopy (TEM) was carried out using a JEOL 3011, 300 kV instrument with a UHR polepiece. The samples for TEM were prepared by dropping the dispersion on amorphous carbon films supported on a copper grid and dried in ambience. Scanning electron microscopic (SEM) images were taken in a HITACHI S-4800 FE-SEM. For the infrared spectra,

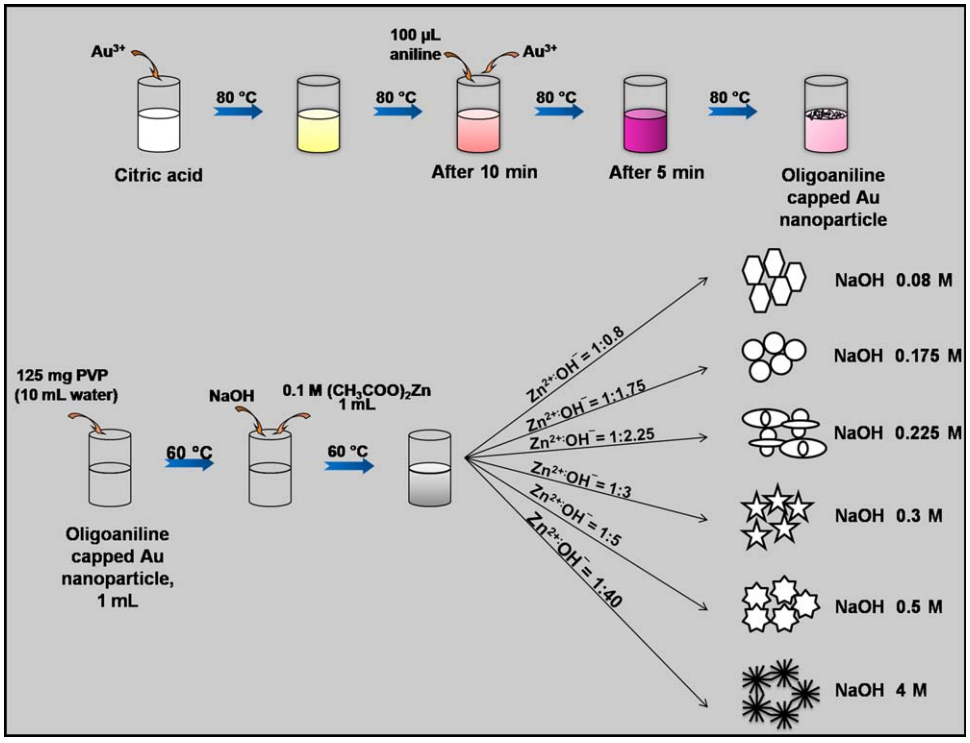

Scheme 1. Procedure used for the synthesis of various anisotropic zinc oxide nanostructures using Au/PANI.

vacuum-dried samples were made in the form of KBr pellets and the spectra were measured with a Perkin-Elmer spectrum one Fourier-transform infrared (FTIR) spectrometer. X-ray diffraction (XRD) data were collected with a Shimadzu XD-D1 diffractometer, using Cu Kα radiation ($\lambda = 1.54$ Å). The samples were scanned in the 2θ range of 10–90°. The Raman Spectra were measured using a confocal Raman spectrometer equipped with an argon ion laser (excitation wavelength 532 nm). Fluorescent spectra were measured using a Nano Log HORIBA JOBIN YVON spectrofluorimeter.

3. Results and discussion

All the nanostructures were synthesized from the PVP-coated Au/PANI precursors. Apart from PVP and Au-oligoaniline precursor concentrations, the ratio of Zn^{2+}:OH^- was the main parameter controlling the morphologies of the prepared nanostructures. Temperature was also seen to affect this template-assisted synthesis.

3.1. Low OH^- concentration (Zn^{2+}:OH^- = 1:0.8, 1:1.75, 1:2.25)

Fig. 1a shows hexagonally shaped plates obtained from a very low ratio of Zn^{2+}:OH^- (1:0.8). These structures have an average diameter of 300 nm. Due to small size of these particles, it is difficult to make out clearly the edges in the shown SEM images. From the high resolution TEM image, it is clear that these are made up of many particles assembled together (Fig. 1b). Particles have a lattice spacing of 0.28 nm, corresponding to the $(10\bar{1}0)$ planes in the ZnO crystal lattice. Slightly increasing the ratio, oval-shaped structures were obtained (Fig. 1c) with high resemblance to the hexagonal plates, having similar lattice spacing as of them, but slightly larger in size. With still higher ratio, certain projections were obtained on these plates (Fig. 1d).

3.2. Medium OH^- concentration (Zn^{2+}:OH^- = 1:3, 1:5, 1:7.5)

Fig. 2b depicts a single star-shaped structure obtained from a ratio of Zn^{2+}:OH^- of 1:3. ZnO stars formed have few arms ranging from 5 to 7, which grew radially from the center. The length of each arm is around 400 nm, the diameter ranging from 25 nm at the tip to about 200 nm near the center of the stars, as seen in the TEM images (Figs. 2b and d). The overall diameter of these structures is around 1 μm. These star-shaped structures have a tendency to cling together (Figs. 2a and c). As the objects are three-dimensional, the two-dimensional projection as in a TEM did not reveal the shape clearly.

Figs. 3a and b show the typical SEM images of the ZnO flower-like structures with multilayered petals. These images reveal the presence of large quantities of uniform-shaped flower-like structures with an average size of 1 μm. The number of petals varies from 20 to 30 and each one exhibits the tapering feature with a center size of 300–500 nm and a tip size of 30–50 nm. Figs. 3c and d present representative TEM micrographs of these flowers. The tip structure of the petal shown in the inset of Fig. 3d indicates that each petal is not a single-crystal, but an assembly of several nanoparticles. The HRTEM image clearly identifies the (0 0 0 2) lattice plane of hexagonal ZnO, with a lattice spacing of 0.26 nm.

With still higher concentration of NaOH (Zn^{2+}:OH^- = 1:7.5), thorn-shaped structures were obtained. These have an average diameter of 1 μm. The edges of these structures were found to

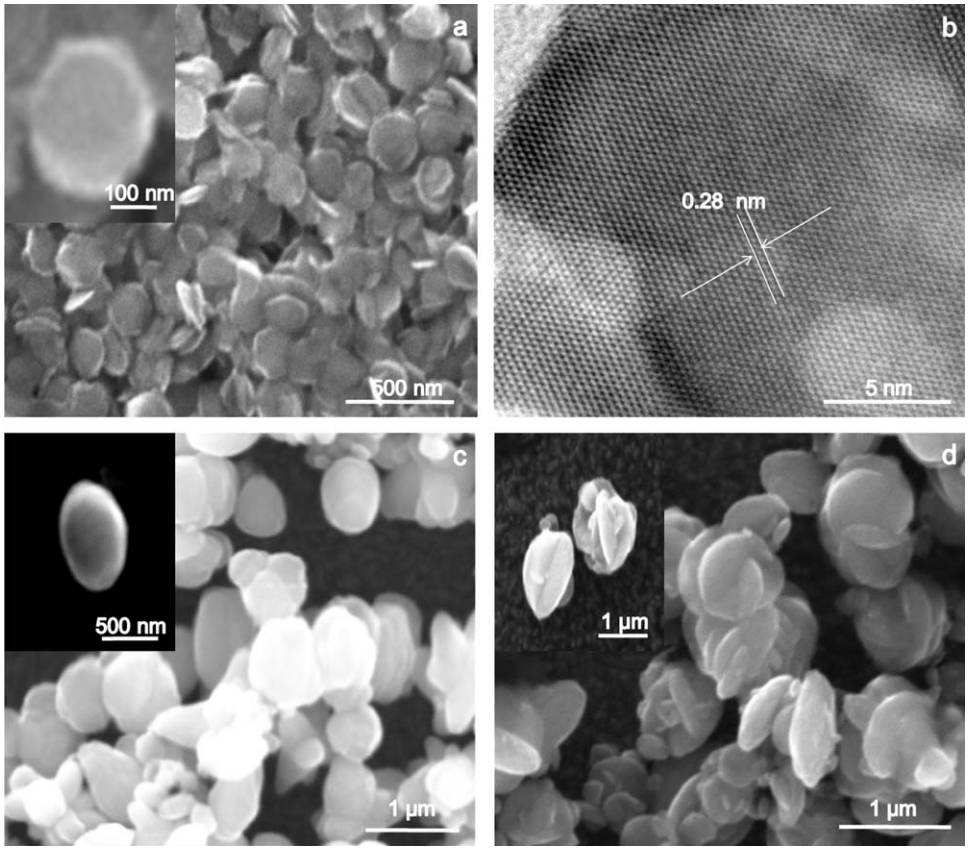

Fig. 1. (a) Large area SEM image of hexagonal plates. Enlarged SEM image of a hexagonal plate is in the inset; (b) high-resolution TEM image of the tip of a hexagonal plate; (c) large-area SEM image of the spheres. SEM image of a sphere is shown as inset; and (d) large-area SEM images of branched plates obtained at higher concentration of NaOH. Inset shows the small-area SEM image of these structures.

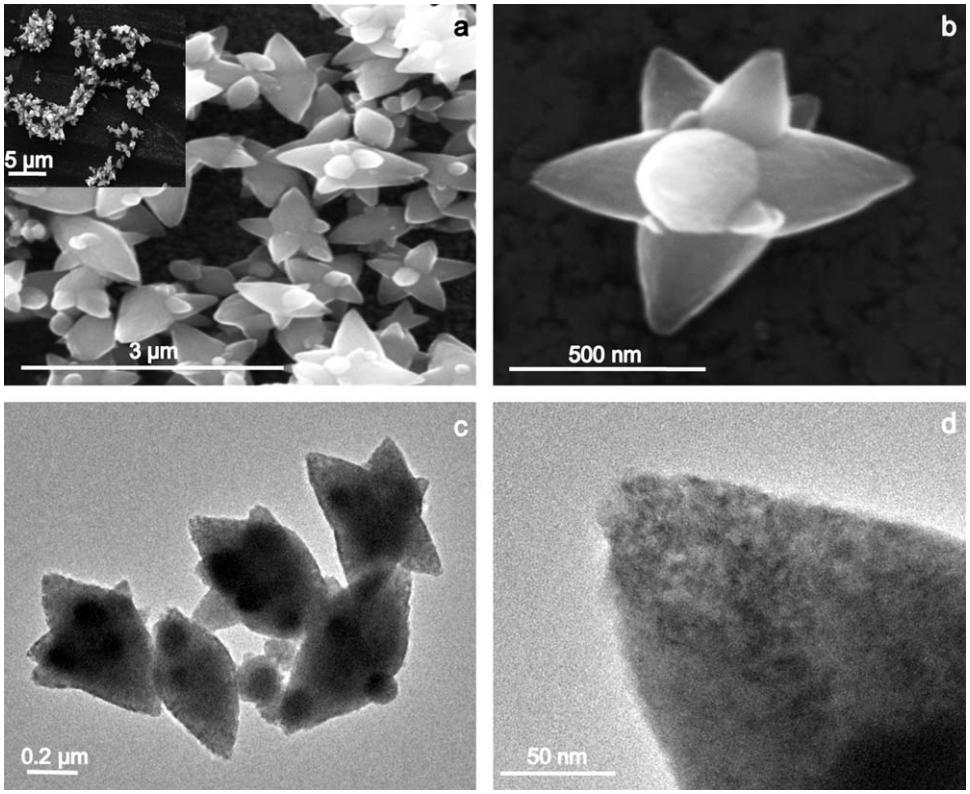

Fig. 2. (a) Large area SEM image of the star structure. The clinging tendency of these structures is shown in the inset; (b) SEM image of a single star; (c) large area TEM image of the star structure; and (d) TEM image of a single tip.

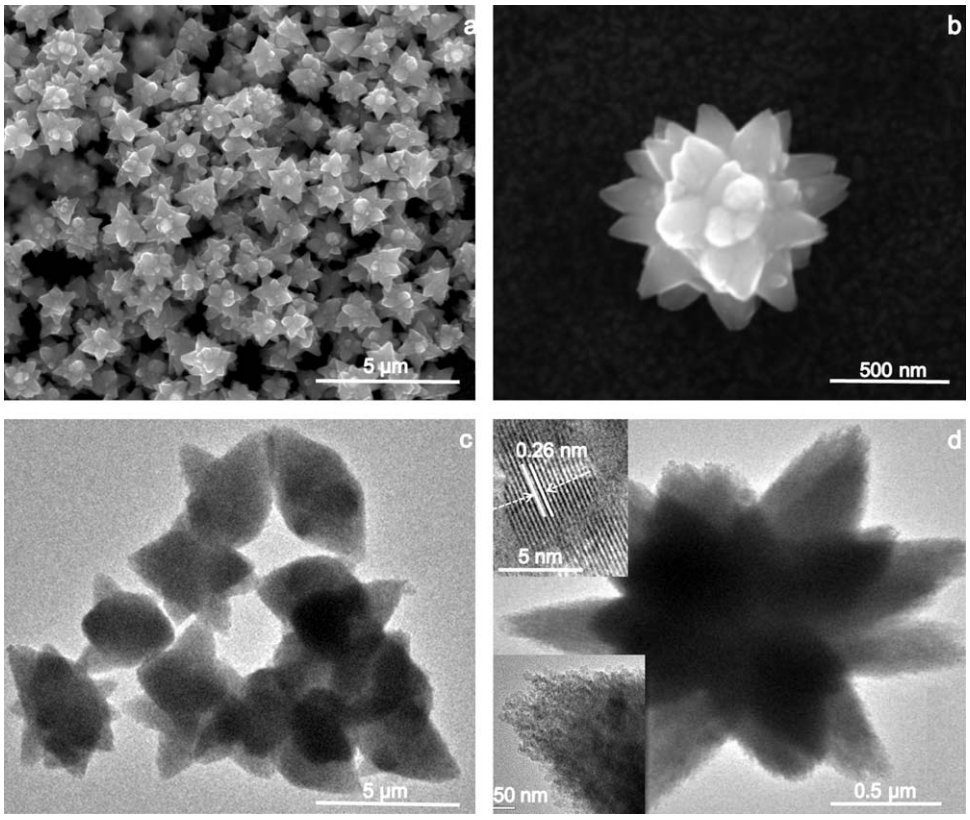

Fig. 3. (a) Large-area SEM image of the microflowers; (b) SEM image of a single flower; (c) and (d) large-area and small-area TEM images of the microflowers. TEM image of the tip and its corresponding HRTEM are inserted as the bottom and top insets, respectively.

have sharp tips of 70 nm diameter (Supplementary information Fig. S1).

3.3. High-OH^- concentration (Zn^{2+}:OH^- = 1:40)

Fig. 4a shows the low-magnification SEM image of the multipods. It reveals that the number of arms varies between 10 and 25 and all have a common origin with almost equal length and breadth of 0.5 and 1 μm, respectively. Fig. 4b shows the SEM image of a single multipod of average length of 1–2 μm. Each multipod is composed of submicrometer-sized rods, which form radiating structures. The inset of Fig. 4b shows the tip of an arm ending in a hexagonal pattern. Fig. 4c shows the low-magnification TEM image of multipods. The inset of Fig. 4d shows the tip of an arm of the multipod having a diameter of 70 nm. From the low-magnification SEM and TEM images (Figs. 4a and c), it is seen that these structures have a tendency to cling to each other forming chains of multipods.

To check the effect of seed on the synthesis, similar experiments were conducted in the absence of seed solution with the other conditions being the same. It was seen that at a low Zn^{2+}:OH^- ratio of 1:0.8, rods obtained were of a few micrometers in length unlike hexagonal plates, seen in the presence of seed solution. The rod thickness was found to vary from 200–500 nm. Even when the ratio of Zn^{2+}:OH^- was increased to 1:2.5, rods seen were of the order of 10–20 μm. But along with this, long chain of ZnO structures with rod-shaped branches were noticed (inset of Supplementary information Fig. S2b). However, at ratios of Zn^{2+}:OH^- = 1:5, similar flower-shaped structures were attained indicating no change with or without seed solution. With extremely large concentration of OH^-, flower-shaped structures were still observed having a length of 3 μm. The tapering nature was no longer visible and each branch of the flower had many rods assembled together, as shown in Supplementary information Fig. S2d.

The EDAX spectra and the corresponding elemental analysis of both star and multipod are shown in Fig. 5 and Supplementary information Fig. S3, respectively. The major elements are Zn and O with no significant amount of Au.

The vibrational properties and phase purity of the ZnO particles prepared at different OH^- concentrations were investigated using the Raman spectroscopy (Fig. 6a). The Raman spectra show the same peaks for all of the ZnO structures. The preeminent E_2 (high) mode at 428 cm^{-1} of bulk ZnO occurs in the sample with minor shifts, supporting the wurtzite phase.

The peaks at 372 and 393 cm^{-1} signifies A_1-(TO) and E_1-(TO) phonons of ZnO crystal, respectively. The peak located at 327 cm^{-1} may be attributed to a multiphonon scattering process of the second E_2 mode. A_1-(LO) and E_1-(LO) modes occur at 556 cm^{-1} and indicates various crystal defects such as oxygen vacancy, zinc interstitials or presence of its complexes. Comparatively, the A_1-(LO) and E_1-(LO) peaks at 556 cm^{-1} were weak showing high crystallinity of the prepared ZnO samples.

The FTIR spectrum of ZnO samples shown in Fig. 6b reveals a series of absorption peaks from 400 to 4000 cm^{-1}. The broad band at 3392 cm^{-1} is due to the O–H stretching vibration of the hydroxyl group. Peaks between 2800 and 3000 cm^{-1} are due to C–H stretching of the alkane groups. The peaks observed at 1647 and 1570 cm^{-1} are due to the asymmetrical and symmetrical stretching of the zinc carboxylate, respectively. The peak at 543 cm^{-1} is due to the O–H bending of the hydroxyl group. The carboxylate probably comes from the adsorption of sodium (zinc) acetate on the surface of the ZnO particles and the hydroxyl results from the hygroscopic nature of ZnO.

ZnO is reported to show two emission bands, an ultraviolet emission band and another in the blue green region. The UV band

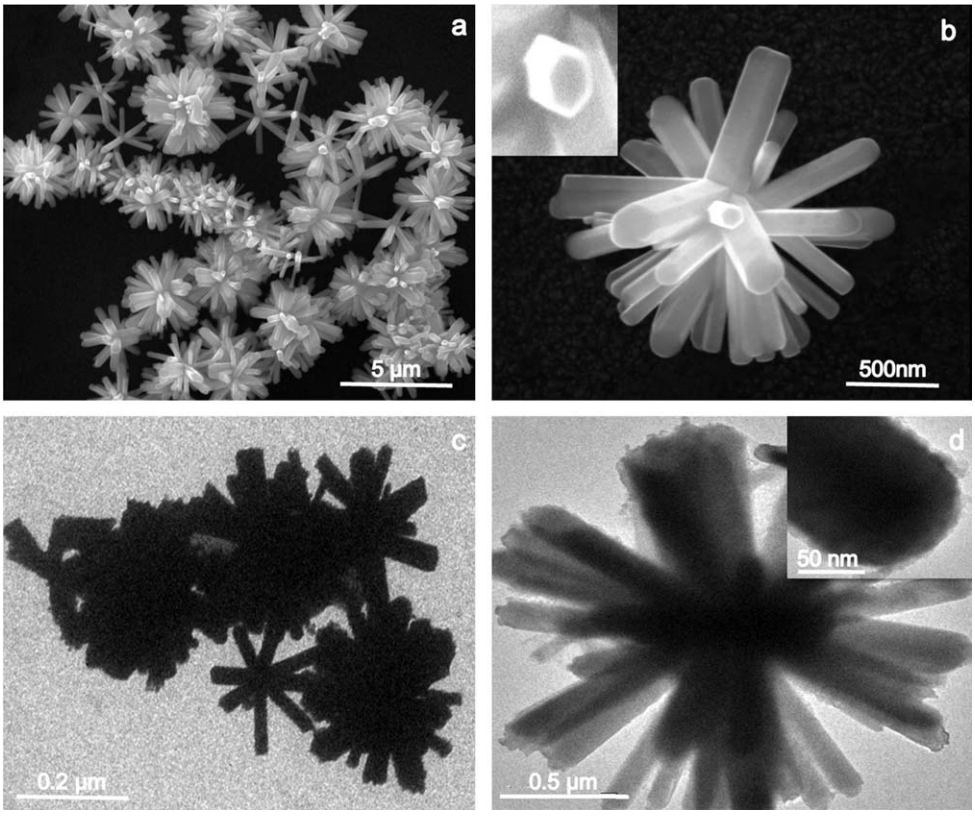

Fig. 4. (a) Large-area SEM image of the multipods; (b) SEM image of a single multipod; (c) and (d) large-area and small-area TEM images, respectively, of the multipods. TEM image of a tip is shown in the inset of d.

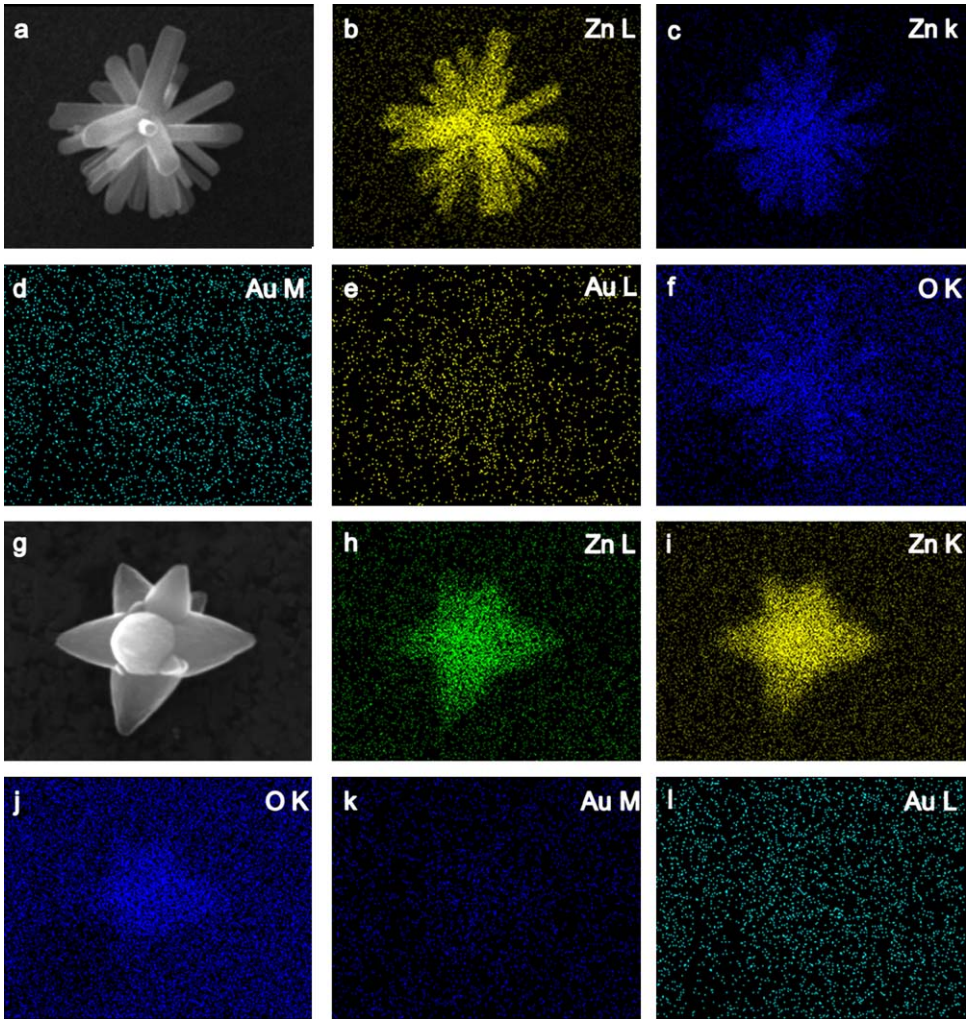

Fig. 5. Insets b–f and h–l shows the EDAX spectra of multipods and stars, respectively. The SEM images of both these structures are shown in a and g.

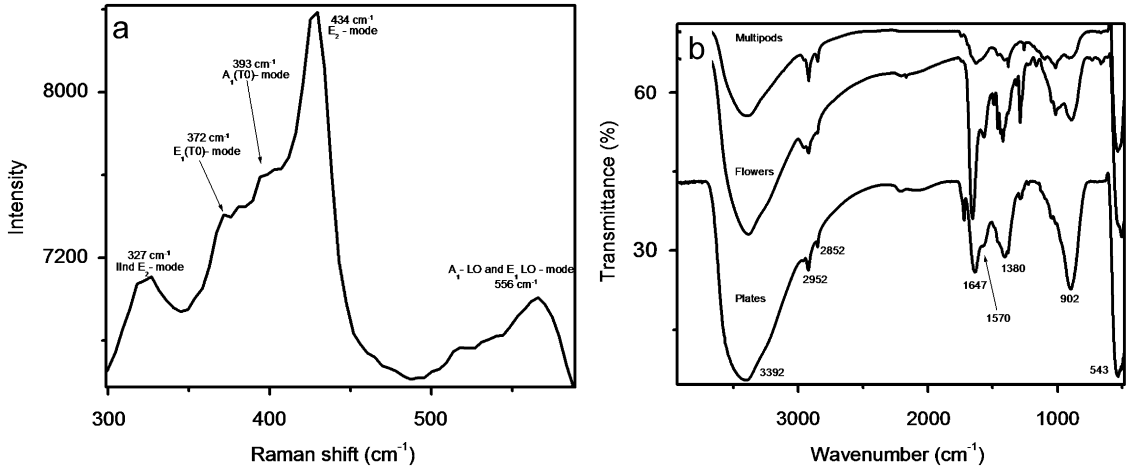

Fig. 6. (a) Raman spectra of the star-shaped zinc oxide structure synthesized using Au oligoaniline. The Raman spectra of different structures showed similar features; (b) FT-IR spectrum of hexagonal plates, flower and multipods shown from bottom to top, respectively.

is commonly associated with the near band edge emission and the blue green band is attributed to defect-related transitions. All the structures obtained showed similar spectra. Supplementary information Fig. S4 presents one such fluorescent spectrum of flower-like zinc oxide supernatant solution. The spectra show an emission band at ~443 nm (due to electron–hole recombination) for excitation at ~353 nm. The blue green fluorescence exhibited by the sample can be easily seen under UV light (inset of Supplementary information Fig. S4).

Fig. 7 shows the powder X-ray diffraction pattern of ZnO nanoparticles taken at low concentration of OH^- (hexagonal plates and spheres), medium concentration of OH^- (star

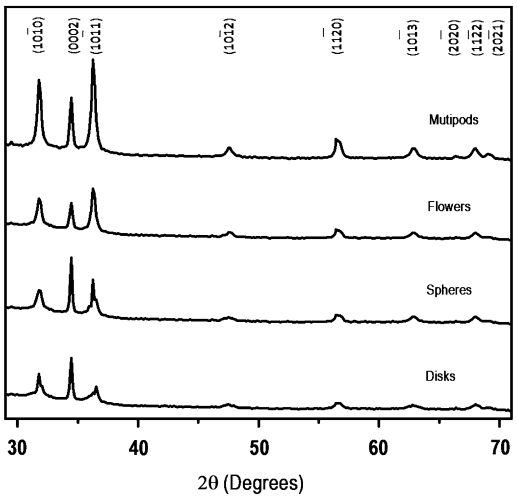

Fig. 7. XRD patterns of hexagonal disks, spheres, flowers and multipods.

structure) and high concentration of OH^- (multipods). Three notable ZnO peaks i.e., (10$\bar{1}$0), (0002) and (10$\bar{1}$1), appear at $2\theta = 31.86^\circ$, 34.68° and 36.36°, respectively, which reveals that ZnO has a crystalline hexagonal wurtzite structure. In the case of hexagonal plates, the crystal size of the ZnO powders was calculated by the Scherrer formula [$D = 0.9\ \lambda/\beta\cos\theta$, where D is crystallite size, λ is the wavelength of the X-rays (1.54 Å), β is the full-width at half maximum intensity of the peak and θ is the diffraction angle]. It gave particle diameters of 2.76 and 2.83 nm, when measured using peak widths at 48.3° and 56.7°, respectively. These values are in good agreement with the TEM estimates of the particle diameter which is 2.8 nm.

From the XRD data (Supplementary information Table. S1), it is seen that in the case of disk-shaped nanostructures, there is a considerable decrease in the peak of (11$\bar{2}$0), (11$\bar{2}$2), (20$\bar{2}$1) and (10$\bar{1}$2) planes with respect to the bulk ZnO and plane (0002) shows maximum intensity unlike bulk ZnO. But when it comes to spheres, though (0002) still retains the maximum peak intensity, it is more amplified than the case of disks. An enhancement of the intensity of (10$\bar{1}$0) plane is seen with a slight decrease in intensity of (10$\bar{1}$1) plane. In the case of flowers and multipod, the 100% peak shifts to (10$\bar{1}$1), similar to bulk ZnO. Also intensity of (0002) plane reduces to less than (10$\bar{1}$0) plane. For the case of flower-shaped structures, an increase in peak intensity of (20$\bar{2}$0) plane is also noticed. A spectacular increase in intensity of (0002) and (10$\bar{1}$0) peaks are seen for multipods. Thus as the pH goes on increasing, a decrease in intensity of (0002) peak with an increase in intensity of (10$\bar{1}$1) is noticed along with slight increase in intensity of (10$\bar{1}$0) plane. The preferential enhancement is in agreement with the structures observed.

Similar reactions were performed under identical reaction conditions with varying temperatures to check its effect on the experimental process as well as on the shape and size of the structures formed. It was seen that changing the temperature neither affects significantly the morphology of these structures nor the ease of decomposition of $Zn(OH)_2$ to ZnO. Three sets of experiments were conducted—one at low temperature of 30 °C, one at actual reaction temperature of 60 °C and the remaining at a slightly higher temperature of 90 °C. The reaction that took place at 30 °C proceeded at slightly slower rate and took a bit more time to complete (2 h), when compared to the reaction that proceeded at 90 °C which took only 40 min to complete. Thus, variation of temperature only slightly affected the rate of the reaction.

Under the reaction conditions, zinc acetate produces Zn^{2+} cations which readily reacts with OH^- anions forming the basic growth unit, $[Zn(OH)_4]^{2-}$. These tetrahedral $[Zn(OH)_4]^{2-}$ ions then decompose to generate ZnO molecular species.

$$Zn^{2+} + 4OH^- \rightarrow [Zn(OH)_4]^{2-} \quad (1)$$

$$[Zn(OH)_4]^{2-} \rightarrow ZnO + H_2O + 2OH^- \quad (2)$$

When NaOH solution was added, a white precipitate of insoluble $Zn(OH)_2$ was formed immediately, which later became a clear solution of $[Zn(OH)_4]^{2-}$ on further heating. Increasing the OH^- content helps to make the solution clearer and ease the formation of ZnO. But with extremely high ratios of OH^-:Zn^{2+} initially, ZnO was not formed even after prolonged reaction. This can be due to the amphoteric characteristics of ZnO, where the rate of formation is less than the rate of dissolution (reverse of reaction (2)).

A possible growth mechanism for the formation of these structures can be explained on the basis of the structure of ZnO. ZnO exhibits a hexagonal wurtzite structure consisting of planes of tetrahedrally coordinated O^{2-} and Zn^{2+} ions, mounded alternately along the polar *c*-axis. The well-developed crystal faces of ZnO evince positively charged polar (0001)-Zn surfaces, six symmetric nonpolar {10$\bar{1}$0} planes of the side facets and negatively charged (000$\bar{1}$)-O polar surfaces [46]. The crystal growth rate in different directions generally follows the order [0001] > [10$\bar{1}$1] > [10$\bar{1}$0] [47]. So the growth nuclei formed in the initial growth stage of ZnO crystals has more chances to grow along the [0001] direction. Further, PVP has a tendency to selectively adsorb on the {1010} planes of the six symmetric side facets of the growth nuclei, allowing growth to occur only along the polar axis [48]. So in the absence of seed solution, rod-like structures were obtained. In the presence of seed solution, there was suppression of the (0001) intensity revealing that Au-oligoaniline act different from PVP, inhibiting growth along the *c*-direction, forming hexagonal shaped disks (preferential equatorial growth). When the OH^- content was increased in the absence of the seed solution, more growth units, $[Zn(OH)_4]^{2-}$ can be generated which leads to rods of increased length with certain branches projecting from it at certain regions. ZnO is an unusual material with the tendency to form fourlings consisting of four acicular spines with a common base and approximately the same angle between them [49]. Fuller deduced that the ZnO particles twinned along the (11$\bar{2}$2) planes produce these so-called fourlings [50]. Each spine of the fourling is a ZnO crystal, elongated along the *c*-axis. Thus, when seed solution was added and as crystals grow, ZnO may twin along the plane to form such fourling-like structures. This is indicated by the considerable change in the (11$\bar{2}$2) peak in the XRD pattern when compared to bulk ZnO. Though these spines readily grow along the polar axis, the seed solution may act as a barrier between the growth nuclei and the polar surface, suppressing multiple nanorod growth along the radial directions from center nuclei, and allowing only isotropic growth leading to sphere-like ZnO crystals. It is believed that thin sheets can form between spines, with each sheet lying in the plane of two spines [51]. These sheets can then act as nuclei for further spines to grow. However, many deviations from this structure can occur resulting in less or more number of spines. So with further increase in OH^- content, due to deviations from this idealized fourling structure, a large number of polar axis-oriented spines may form, resulting in flower-shaped ZnO crystals. The fourling is further shown by the symmetry of the structures obtained having almost similar angles between the spines. The tapering of these spines along the length is due to the increased dissolution rates beyond a certain OH^- concentration. Here, the low concentration of seed may not be enough to completely

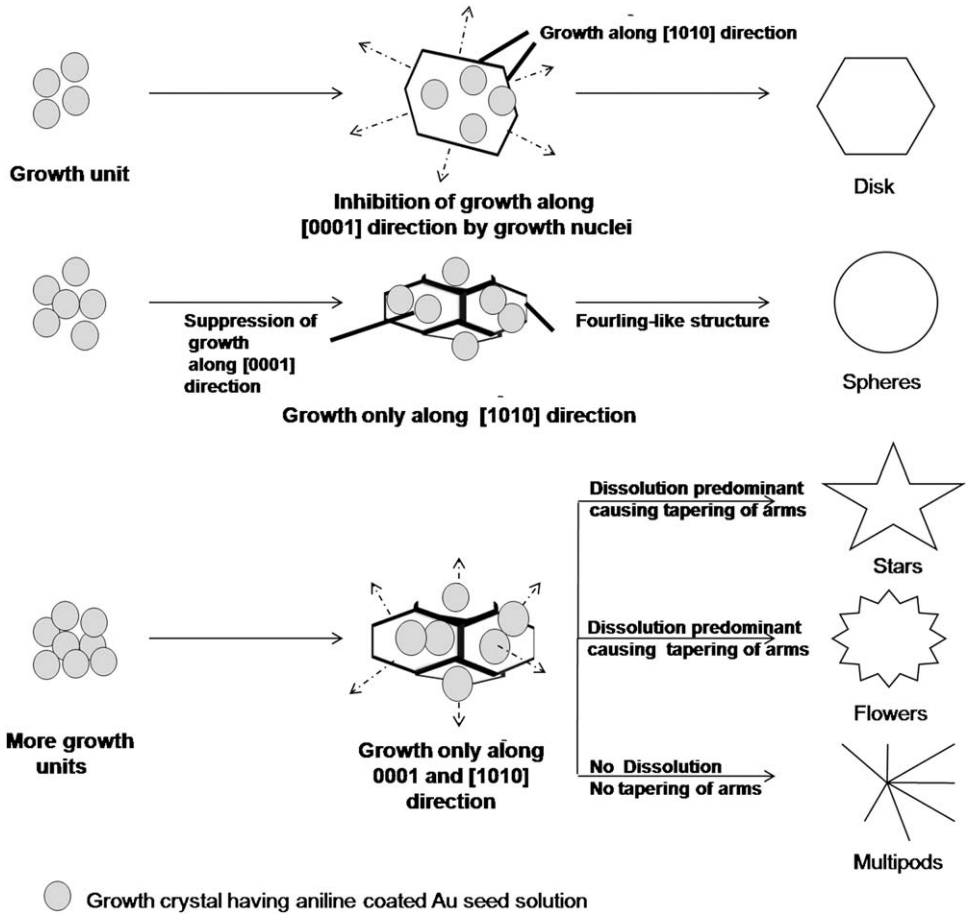

Fig. 8. Schematic representation of the growth of various ZnO nanostructures using Au–oligoaniline seeds.

suppress the elongation of the polar axis. So spine growth was seen in certain regions resulting in identical structures with and without the seed solution. But a slight decrease in the number of spines was observed in the presence of seed solution, due to its inhibitory action on the polar surface. At extremely large concentration of OH^-, more than enough growth units may be available to overcome the decrease, due to dissolution and so no tapering was observed. In the absence of seed solution, arms seem to generate from the center of each of the facets. These arms contain many rods, placed close to each other, showing high affinity between these rods to join together. But in the presence of seed solution, the rods are much smoother and are of more uniform length and also do not seem to have much affinity among themselves indicating that the seed solution inhibits the tendency of various rods to attach towards each other. Fig. 8 shows the schematic representation of the growth mechanism of these structures.

4. Conclusions

A set of highly crystalline zinc oxide structures, such as disks, spheres, stars, flowers, thorns and multipods were selectively synthesized by a template-assisted seed-mediated approach using oligoaniline-coated gold nanoparticle precursors. In the absence of the seed solution, a different set of structures were obtained at low- and high-OH^- concentrations, but at a ratio of Zn^{2+}:OH^- of 1:5, almost similar structures were seen as in the presence of seed solution. Apart from the seed and oligoaniline concentrations, the OH^- content was the main parameter controlling the morphologies of these structures. Different morphologies can be obtained by selectively capping or passivating certain specific planes as well as by controlling the concentration of the growth nuclei. Dissolution of growth units was also seen to bring changes to these morphologies. A growth mechanism has been proposed based on the XRD data of the various structures. SEM, TEM, Raman, FTIR and fluorescence spectroscopies were utilized for the characterization of the prepared structures. This route offers a fast and low-temperature approach for the synthesis of a wide range of zinc oxide nanostructures.

Acknowledgement

We thank Department of Science and Technology, Government of India for constantly supplementary our research program on nanomaterials.

Appendix. Supporting information

Supplementary data associated with this article can be found in the online version at doi:10.1016/j.jcrysgro.2009.06.019.

References

[1] M.H. Huang, S. Mao, H. Feick, H. Yan, Y. Wu, H. Kind, E. Weber, R. Russo, P. Yang, Science 292 (2001) 1897.
[2] L. Vayssieres, K. Keis, A. Hagfeldt, S.E. Lindquist, Chem. Mater. 13 (2001) 4395.
[3] R. Konenkamp, L. Dloczik, K. Ernst, C. Olecsh, Physica E 14 (2002) 219.

[4] D.M. Bagnall, Y.F. Chen, Z. Zhu, T. Yao, S. Koyama, M.Y. Shen, T. Goto, Appl. Phys. Lett. 70 (1997) 2230.
[5] H. Cao, J.Y. Xu, D.Z. Zhang, S.H. Chang, S.T. Ho, E.W. Seelig, X. Liu, R.P.H. Chang, Phys. Rev. Lett. 84 (2000) 5584.
[6] M.H. Huang, S. Mao, H. Feick, H. Yan, Y. Wu, H. Kind, E. Weber, R. Russo, P. Yang, Science 292 (2001) 1897.
[7] X. Duan, Y. Huang, R. Agarwal, C.M. Lieber, Nature 421 (2003) 241.
[8] Q. Wan, Q.H. Li, Y.J. Chen, T.H. Wang, X.L. He, J.P. Li, C.L. Lin, Appl. Phys. Lett. 84 (2004) 3654.
[9] Y. Darici, P.H. Holloway, J. Sebastian, T. Trottier, S. Jones, J.J. Rodriquez, Vac. Sci. Technol. 17 (1999) 692.
[10] Y. Lu, I.A. Dajani, R.J. Knize, Electron. Lett. 42 (2006) 1309.
[11] M. Law, L. Greene, J.C. Jonhnson, R. Saykally, P. Yang, Nat. Mater. 4 (2005) 455.
[12] Y. Cui, Z. Zhong, D. Wang, W.U. Wang, C.M. Lieber, Nano Lett. 3 (2003) 149.
[13] B.S. Kang, F. Ren, Y.W. Heo, L.C. Tien, D.P. Norton, S.J. Pearton, Appl. Phys. Lett. 86 (2005) 112105.
[14] K. Tominaga, N. Umezu, I. Mori, T. Ushiro, T. Moriga, I. Nakabayashi, Thin Solid Films 334 (1998) 35.
[15] T. Minami, S. Ida, T. Miyata, Y. Minamino, Thin Solid Films 445 (2003) 268.
[16] C.X. Xu, X.W. Sun, Z.L. Dong, M.B. Yu, Appl. Phys. Lett. 85 (2004) 3878–3880.
[17] Y.C. Kong, D.P. Yu, B. Zhang, W. Fang, S.Q. Feng, Appl. Phys. Lett. 78 (2001) 407–409.
[18] Z.W. Pan, Z.R. Dai, Z.L. Wang, Science 291 (2001) 1947–1949.
[19] B.P. Zhang, N.T. Binh, K. Wakatsuki, Y. Segawa, Y. Yamada, N. Usami, M. Kawasaki, H. Koinuma, Appl. Phys. Lett. 84 (2004) 4098–4100.
[20] B. Daudin, J.L. Rouviere, M. Arlery, Appl. Phys. Lett. 69 (1996) 2480.
[21] P.X. Gao, Z.L. Wang, J. Am. Chem. Soc. 125 (2003) 11299–11305.
[22] S. Bhattacharya, A.K. Das, A. Banerjee, D.J. Chakravorty, Phys. Chem. B 110 (2006) 10757–10761.
[23] Z.P. Zhang, X.Q. Shao, H.D. Yu, Y.B. Wang, M.Y. Han, Chem. Mater. 17 (2005) 332–336.
[24] Z.R. Tian, J.A. Voigt, J. Liu, B. McKenzie, M.J. McDermott, M.A. Rodriguez, H. Konishi, H.F. Xu, Nat. Mater. 2 (2003) 821.
[25] G.Z. Shen, D. Chen, K.B. Tang, F.Q. Li, Y.T. Qian, Chem. Phys. Lett. 370 (2003) 334–337.
[26] H. Deng, X.L. Li, Q. Peng, X. Wang, J.P. Chen, Y.D. Li, Angew. Chem. Int. Ed. 44 (2005) 2782–2785.
[27] J.Y. Lao, J.Y. Huang, D.Z. Wang, Z.F. Ren, Nano Lett. 3 (2003) 235.
[28] B.Q. Cao, W.P. Cai, F.Q. Sun, Y. Li, Y. Lei, L.D. Zhang, Chem. Commun. 14 (2004) 1604–1605.
[29] X.Y. Kong, Z.L. Wang, Nano Lett. 3 (2003) 1625.
[30] H. Zhang, D. Yang, Y. Ji, X. Ma, J. Xu, D.J. Que, Phys. Chem. B 108 (2004) 3955.
[31] H. Zhang, D.R. Yang, X.Y. Ma, Y.J. Ji, J. Xu, D.L. Que, Nanotechnology 15 (2004) 622–626.
[32] L.S. Zhang, J.S. Hu, H.P. Liang, A.M. Cao, W.G. Song, L.J. Wan, Adv. Mater. 18 (2006) 2426–2431.
[33] M.S. Arnold, P. Avouris, Z.W. Pan, Z.L.J. Wang, Phys. Chem. B 107 (2003) 659.
[34] Y.C. Kong, D.P. Yu, B. Zhang, W. Fang, S.Q. Feng, Appl. Phys. Lett. 78 (2001) 407–409.
[35] W.L. Hughes, Z.L. Wang, Appl. Phys. Lett. 82 (2003) 2886.
[36] Z.W. Pan, Z.R. Dai, Z.L. Wang, Science 291 (2001) 1947–1949.
[37] W.I. Park, D.H. Kim, S.W. Jung, G.C. Yi, Appl. Phys. Lett. 80 (2002) 4232.
[38] J.B. Baxter, E.S. Aydil, Appl. Phys. Lett. 86 (2005) 053114.
[39] P. Yang, H. Yan, S. Mao, R. Russo, J. Johnson, R. Saykally, N. Morris, J. Pham, R. He, H.J. Choi, Adv. Funct. Mater. 12 (2002) 323.
[40] B.D. Yao, Y.F. Chan, N. Wang, Appl. Phys. Lett. 81 (2002) 757.
[41] C.K. Xu, G.D. Xu, Y.K. Liu, G.H. Wang, Solid State Commun. 122 (2002) 175.
[42] L. Vayssieres, Adv. Mater. 15 (2003) 464.
[43] M.S. Tokumoto, S.H. Pulcinelli, C.V. Santilli, V.J. Briois, Phys. Chem. B 107 (2003) 568.
[44] P.R. Sajanlal, T.S. Sreeprasad, A.S. Nair, T. Pradeep, Langmuir, 24, 9, 2008, 4607, 4614, P.R. Sajanlal, T. Pradeep, Nano Res. 2 (2009) 306.
[45] S. Gao, H. Zhang, X. Wang, R. Deng, D. Sun, G. Zheng, J. Phys. Chem. B 110 (2006) 15847.
[46] S. Komarneni, M. Bruno, E. Mariani, Issue Series Title: Mater. Res. Bull. 35 (2000) 1843.
[47] A. Wei, X.W. Sun, C.X. Xu, Z.L. Dong, Y. Yang, S.T. Tan, W. Huang, Nanotechnology 17 (2006) 1740.
[48] K. Biswas, B. Das, C.N.R. Rao, J. Phys. Chem. C 112 (7) (2008) 2404–2411.
[49] S.W.K. Morgan, Zinc and Its Alloys and Compounds, EllisHorwood Ltd., Chichester, England, 1985.
[50] M.N. Fuller, J. Appl. Phys. 15 (1944) 164.
[51] R.A. McBride, J.M. Kelly, D.E. McCormack, J. Mater. Chem. 13 (2003) 1196.